Biological Psychiatry: Celebrating 50 Years

Archival Report

Postnatal *Tshz3* Deletion Drives Altered Corticostriatal Function and Autism Spectrum Disorder–like Behavior

Dorian Chabbert, Xavier Caubit, Pierre L. Roubertoux, Michèle Carlier, Bianca Habermann, Bernard Jacq, Pascal Salin, Mehdi Metwaly, Christina Frahm, Ahmed Fatmi, Alistair N. Garratt, Dany Severac, Emeric Dubois, Lydia Kerkerian-Le Goff, Laurent Fasano, and Paolo Gubellini

ABSTRACT

BACKGROUND: Heterozygous deletion of the *TSHZ3* gene, encoding for the teashirt zinc-finger homeobox family member 3 (TSHZ3) transcription factor that is highly expressed in cortical projection neurons (CPNs), has been linked to an autism spectrum disorder (ASD) syndrome. Similarly, mice with *Tshz3* haploinsufficiency show ASD-like behavior, paralleled by molecular changes in CPNs and corticostriatal synaptic dysfunctions. Here, we aimed at gaining more insight into "when" and "where" *TSHZ3* is required for the proper development of the brain, and its deficiency crucial for developing this ASD syndrome.

METHODS: We generated and characterized a novel mouse model of conditional *Tshz3* deletion, obtained by crossing *Tshz3*$^{flox/flox}$ with *CaMKIIalpha-Cre* mice, in which *Tshz3* is deleted in CPNs from postnatal day 2 to 3 onward. We characterized these mice by a multilevel approach combining genetics, cell biology, electrophysiology, behavioral testing, and bioinformatics.

RESULTS: These conditional *Tshz3* knockout mice exhibit altered cortical expression of more than 1000 genes, ~50% of which have their human orthologue involved in ASD, in particular genes encoding for glutamatergic synapse components. Consistently, we detected electrophysiological and synaptic changes in CPNs and impaired corticostriatal transmission and plasticity. Furthermore, these mice showed strong ASD-like behavioral deficits.

CONCLUSIONS: Our study reveals a crucial postnatal role of TSHZ3 in the development and functioning of the corticostriatal circuitry and provides evidence that dysfunction in these circuits might be determinant for ASD pathogenesis. Our conditional *Tshz3* knockout mouse constitutes a novel ASD model, opening the possibility for an early postnatal therapeutic window for the syndrome linked to *TSHZ3* haploinsufficiency.

Keywords: Autism spectrum disorder, Cortex, Sociability, Stereotypies, Striatum, Synaptopathy

https://doi.org/10.1016/j.biopsych.2019.03.974

The basal ganglia constitute a functional network of subcortical structures playing a crucial role in extrapyramidal motor control and motor learning, as well as in associative learning, planning, working memory, and emotion. The striatum is the main input station of the basal ganglia, receiving major projections coming from layer 5 (L5) cortical projection neurons (CPNs). These corticostriatal glutamatergic afferences contact mainly striatal spiny projection neurons (SPNs), the major neuronal population of this nucleus (1–3). There is accumulating evidence showing altered development and function of corticostriatal circuitry and striatal dysmorphic features in autistic patients (4–10). Autism spectrum disorder (ASD) is a heterogeneous group of neurodevelopmental pathologies characterized by impairments in social communication and interaction, restricted interests, and repetitive behaviors (11). ASD etiology has a strong genetic component, with a high number of genes and factors involved (12–15). Accordingly, abnormal corticostriatal function has also been found in ASD mouse models, such as *Shank3*$^{-/-}$ (16,17), *neuroligin-1*$^{-/-}$ (18), and *16p11*$^{+/-}$ mice (19). In this context, we have recently identified *TSHZ3* (teashirt zinc-finger homeobox family member 3, also known as *ZNF537*) as a susceptibility gene for ASD: patients with heterozygous *TSHZ3* deletion show ASD neurodevelopmental phenotypes including autistic behavior and intellectual disability, and in particular, speech disturbance; renal tract abnormalities are also frequently observed in these patients (20). *TSHZ3* gene codes for the highly conserved, zinc-finger homeodomain transcription factor TSHZ3, whose expression starts during prenatal development in both human and mouse (21). Moreover, *TSHZ3* has been identified in human neocortical gene networks with the highest expression during late fetal development, which have been linked to not only ASD but also other neuropsychiatric disorders and IQ (20,22). *Tshz3*-null mutation in mouse (*Tshz3*$^{-/-}$) leads to

ISSN: 0006-3223

altered expression of cortical layer markers (20) and is lethal at birth (23), suggesting that TSHZ3 plays a critical role during prenatal brain development. Interestingly, heterozygous *Tshz3* deletion in mice ($Tshz3^{+/-}$) faithfully mimics the human disorder, as these animals show reduced sociability, narrowed field of interest, stereotypies, and anxiety, associated with renal tract defects. These ASD-like symptoms are paralleled by altered expression of neocortical gene markers at both embryonic (embryonic day 18.5 [E18.5]) and postnatal (postnatal day 5 [P5] and P20) stages, and by altered function of the corticostriatal pathway (20). However, L5 CPNs, which project to the ipsi- and/or contralateral striatum, express TSHZ3 not only during fetal development, but also postnatally and in adulthood, an expression pattern that is comparable in human and mouse (20,21,24,25). The postnatal development of the corticostriatal circuitry has been little characterized, but studies in animals have shown that its maturation progresses after birth (26–30). Therefore, the postnatal role of TSHZ3 in the maturation and function of the corticostriatal system needs to be elucidated.

For this, we generated a novel conditional mutant mouse with *Tshz3* deletion in CPNs at an early postnatal stage. We show here that this time- and region-specific loss of *Tshz3* results in ASD-relevant behavioral deficits similar to those we previously described in $Tshz3^{+/-}$ mice, which are paralleled by cortical and striatal changes in terms of gene expression, synaptic transmission, and synaptic plasticity. These data suggest that postnatal events might contribute to the *TSHZ3*-linked ASD syndrome, opening perspectives for a possible early therapeutic window.

METHODS AND MATERIALS

Additional methods and materials are provided in Supplement 1.

Generating *Tshz3*-Conditional Knockout Mice

Animal experimental procedures were approved by the Comité National de Réflexion Ethique sur l'Expérimentation Animale 14' (57-07112012) and in agreement with the European Communities Council Directive (2010/63/EU). Conditional mouse mutants with postnatal loss of *Tshz3* in the cortex (hereby referred to as *Tshz3-pnCxKO*) were generated by crossing $Tshz3^{flox/flox}$ mice with *CaMKIIalpha-Cre* that express the CRE-recombinase in glutamatergic CPNs, as described in Supplement 1. Control mice were $Tshz3^{flox/flox}$.

Morphometric and Dendritic Spine Analysis of L5 CPNs

We used transgenic mouse lines (age P28) expressing *Thy1*-green fluorescent protein (GFP) in L5 CPNs (31). *Thy 1-GFP-M;Tshz3-pnCxKO* mice were obtained by crossing *CaMKIIalpha-Cre;*$Tshz3^{flox/flox}$ male mice with $Tshz3^{flox/flox}$ female mice heterozygous for *Thy1-GFP*. Stacks from 100-μm vibratome sections (1-μm z-step) were acquired using a Zeiss LSM780 (Carl Zeiss Meditec, Oberkochen, Germany) laser scanning confocal microscope (40× objective, zoom 0.6). Isolated *Thy1-GFP*-positive L5 CPNs of the primary motor and somatosensory cortex were imaged and reconstructed using the NeuronJ plugin of ImageJ 1.45s (National Institutes of Health, Bethesda, MD) in 2-dimensional projections. All dendrites were semimanually traced and labeled as primary (dendrite originating from the soma), secondary (extending from the primary dendrite), or higher-order dendrites. Fifteen cells were reconstructed for each genotype from 4 littermate pairs of P28 control (*Thy1-GFP-M;*$Tshz3^{flox/flox}$) and mutant (*Thy1-GFP-M;Tshz3-pnCxKO*) mice. Sholl cross-analysis was performed by counting the number of dendrites intersecting concentric spherical radii at 10-μm intervals. Differences at specific radii were analyzed using unpaired Student's *t* test.

Analysis of spine density and morphology was performed on 4 littermate pairs (see above). Images were acquired as described above (63× objective, numerical aperture 1.4, 0.03 μm/pixel, voxel size 0.033 μm^2 × 0.37 μm). Spine counts were obtained from second- or third-order basal dendritic branches of randomly selected L5 CPNs. Dendrites from five to seven cells were analyzed per animal, providing a cumulated dendrite length >750 μm for each genotype. Spine identification and density were evaluated using NeuronStudio (32). Statistical analysis was performed using an unpaired Student's *t* test (BiostaTGV statistical software; http://www.u707.jussieu.fr/

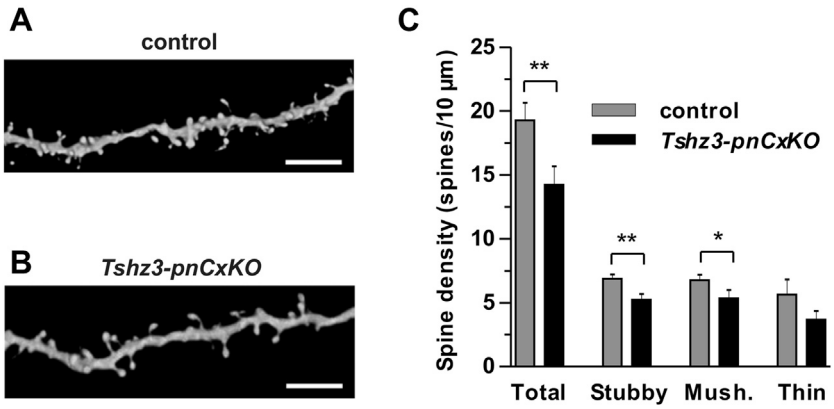

Figure 1. Reduced spine density in conditional mutant mice with postnatal loss of *Tshz3* in the cortex (*Tshz3-pnCxKO*). **(A, B)** Three-dimensional reconstruction of representative confocal images showing dendritic spines of green fluorescent protein–positive layer 5 cortical projection neurons of the primary motor and somatosensory cortex from control and *Tshz3-pnCxKO* mice at postnatal day 28. Scale bar = 5 μm. **(C)** Density of spines in control (gray) and *Tshz3-pnCxKO* (black) mice (mean ± SEM). Data are from 1421 spines over 760-μm dendritic segment length and 1092 spines over 788-μm dendritic segment length, respectively. Decrease: total ∼26% (from 19.26 ± 1.38 spines/10 μm in control mice to 14.24 ± 1.42 spines/10 μm in *Thy1-GFP-M;Tshz3-pnCxKO* mice); stubby ∼24%, (from 6.86 ± 0.36 spines/10 μm in control mice to 5.23 ± 0.46 spines/10 μm in *Thy1-GFP-M;Tshz3-pnCxKO* mice); mushroom (Mush.) ∼21% (from 6.77 ± 0.42 spines/10 μm in control mice to 5.35 ± 0.66 spines/10 μm in *Thy1-GFP-M;Tshz3-pnCxKO* mice); thin ∼34%. *$p < .05$ and **$p < .01$, control vs. *Tshz3-pnCxKO* mice, Mann-Whitney test.

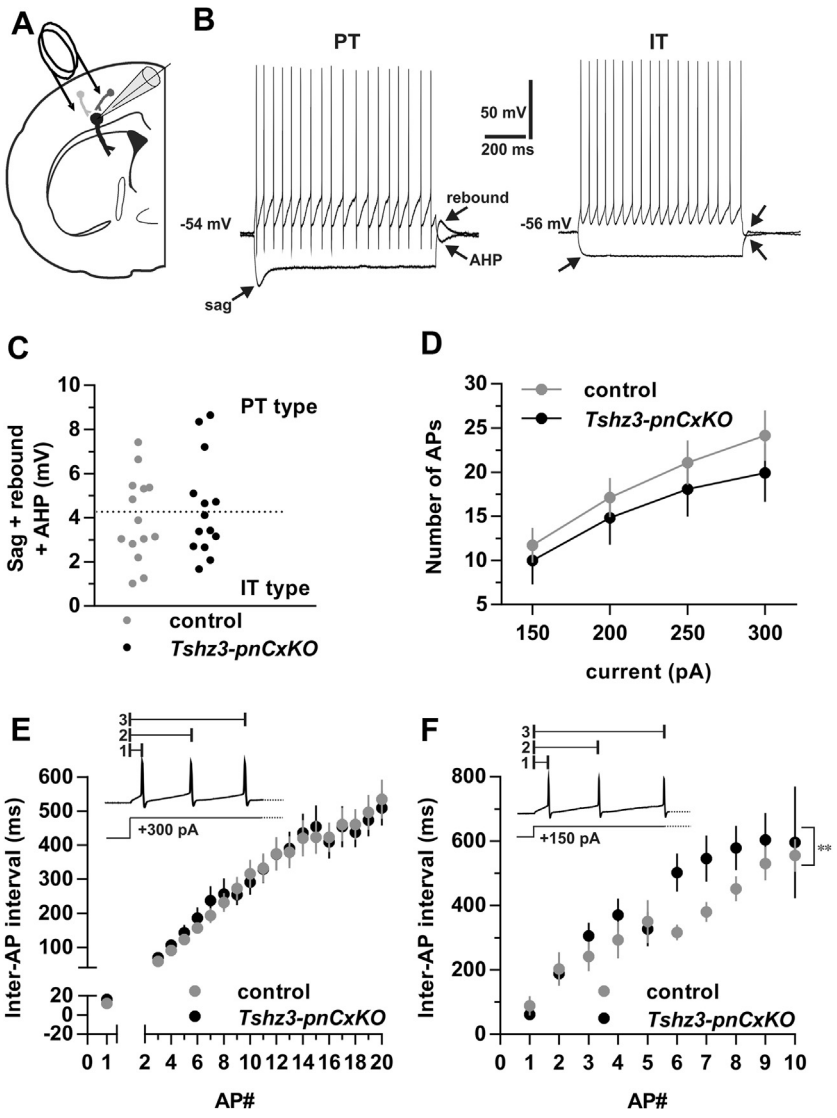

Figure 2. Electrophysiological properties of layer 5 cortical projection neurons (CPNs). **(A)** Scheme of a corticostriatal slice with a layer 2/3 neuron (light gray), a gamma-aminobutyric acidergic interneuron (dark gray), and a layer 5 CPN (black), as well as the stimulating and recording electrodes. **(B)** Sample traces showing the responses to ±200-pA pulses of a pyramidal tract (PT) and an intratelencephalic (IT) CPN recorded from the primary motor and somatosensory cortex [as in panel **(A)**]: note the prominent sag, rebound, and afterhyperpolarization (AHP) of the PT neuron compared with the IT neuron. **(C)** Arbitrary classification of CPNs as PT or IT based on the sum of the sag and rebound in response to a −50-pA current pulse, and the AHP following a +50-pA pulse (both for 800 ms). CPNs are considered as PT if sag + rebound + AHP >4.2 mV (dotted line) and as IT if <4.2 mV. The distribution of sag + rebound + AHP values is similar in control mice and conditional mutant mice with postnatal loss of *Tshz3* in the cortex (*Tshz3-pnCxKO*) (n = 14 for each genotype, p = .765, Mann-Whitney test). **(D)** The number of action potentials (APs) triggered by depolarizing current pulses (800 ms) is similar between control and mutant mice ($F_{1,66}$ = 0.6076, p = .444, matched 2-way analysis of variance). **(E)** The graph shows the delay between the beginning of a depolarizing current pulse (+300 pA, 800 ms) and the first 20 APs triggered (see inset) in CPNs: average values are similar in the two groups (n = 14 for each genotype [$F_{1,436}$ = 0.102, p = .75, two-way analysis of variance]). **(F)** Same as panel **(E)**, but using a smaller current pulse (+150 pA, 800 ms; see inset) just above the average rheobase: *Tshz3-pnCxKO* CPNs show significantly longer inter-AP intervals (n = 14 for each genotype [$F_{1,150}$ = 7.135, p = .008, two-way analysis of variance]). **p = .008. **(D–F)** Data are expressed as mean ± SEM.

biostatgv/) and results considered significant at $p < .05$. Data are expressed as mean ± SEM.

Electrophysiology

Procedures were similar to those described previously (20,33). See also Supplement 1. Acute coronal corticostriatal slices (250-μm thick) from *Tshz3-pnCxKO* and control mice (P21–28) were obtained as previously described (20,33). Whole-cell patch-clamp recordings were performed in oxygenated artificial cerebrospinal fluid at 34°C to 35°C, flowing at ~2.5 mL/min. L5 CPNs of the primary motor and somatosensory cortex and SPNs of the dorsolateral striatum were identified by infrared video microscopy and by their electrophysiological properties (34,35), and were recorded in whole-cell patch-clamp by borosilicate micropipettes (5–6 MΩ) filled with an internal solution containing 125-mM K-gluconate, 10-mM NaCl, 1-mM $CaCl_2$, 2-mM $MgCl_2$, 0.5-mM BAPTA, 19-mM HEPES, 0.3-mM Na-guanosine triphosphate, and 1-mM Mg-adenosine triphosphate, pH 7.3. For *N*-methyl-D-aspartate (NMDA)/alpha-amino-3-hydroxy-5-methyl-4-isoxazole propionic acid (AMPA) ratio experiments, the internal solution contained 140-mM CsCl, 10-mM NaCl, 0.1-mM $CaCl_2$, 10-mM HEPES, 1-mM EGTA, 2-mM Mg-adenosine triphosphate, and 0.5-mM Na-guanosine triphosphate, pH 7.3. For measuring gamma-aminobutyric acidergic (GABAergic) synaptic transmission, the internal solution contained 126-mM mM $CsCH_3SO_3$, 10-mM mM HEPES, 1-mM EGTA, 2-mM QX-314 chloride, 0.1-mM $CaCl_2$, 4-mM Mg-adenosine triphosphate, and 0.3-mM Na-guanosine triphosphate, pH 7.3. A stimulating bipolar electrode was placed either in the cortex at the level of L4 to activate local fibers and evoke glutamatergic excitatory postsynaptic currents (EPSCs) and GABAergic inhibitory postsynaptic currents in L5 CPNs, or in the corpus callosum to

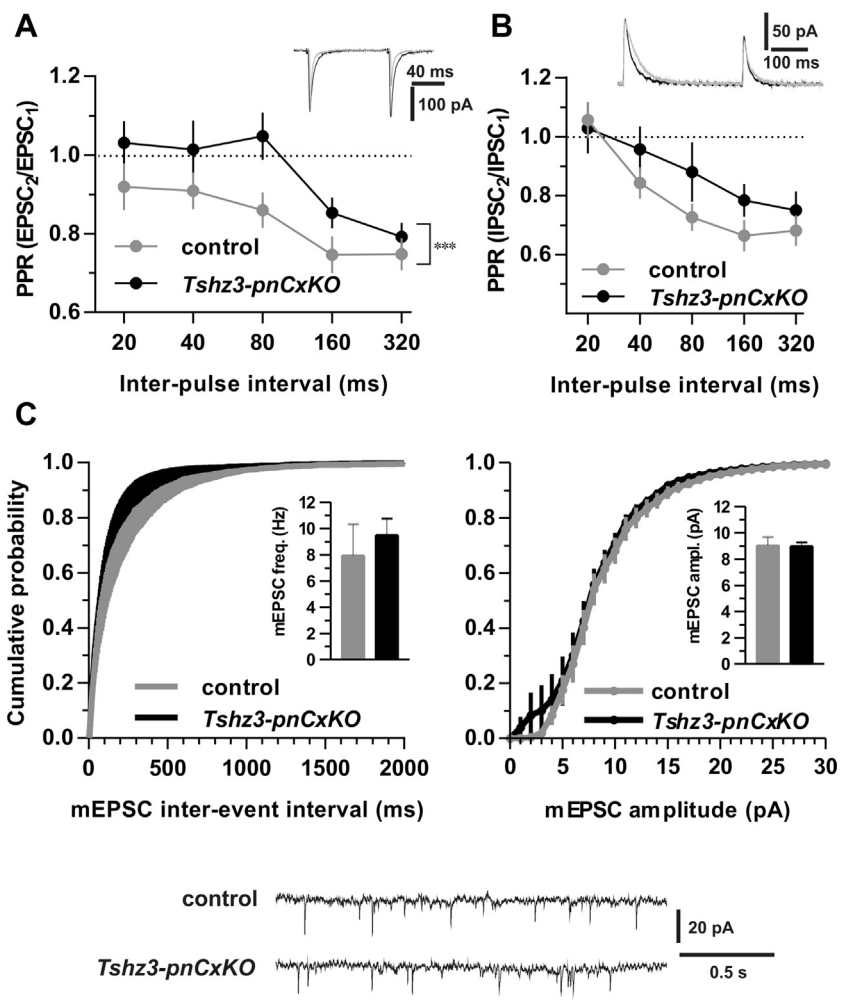

Figure 3. Cortical synaptic transmission. **(A)** The paired-pulse ratio (PPR) of glutamatergic excitatory postsynaptic currents (EPSCs) is significantly higher in cortical projection neurons (CPNs) of conditional mutant mice with postnatal loss of *Tshz3* in the cortex (*Tshz3-pnCxKO*) (n = 29) compared with control mice (n = 22) ($F_{1,241}$ = 10.72, p = .0012, two-way analysis of variance). Traces (inset) depict superimposed EPSCs (amplitude is normalized to control $EPSC_1$) triggered by paired-pulse stimulation recorded from CPNs of control and mutant mice. ***p = .0012. **(B)** The average PPR of gamma-aminobutyric acidergic inhibitory postsynaptic currents (IPSCs) is similar in CPNs of *Tshz3-pnCxKO* (n = 14) and control (n = 10) mice ($F_{1,109}$ = 3.38, p = .069). **(C)** Cumulative distributions of miniature EPSC (mEPSC) interevent interval and amplitude (graphs), as well as frequency and amplitude (insets), are similar in CPNs of control and *Tshz3-pnCxKO* mice. Traces depict sample mEPSCs. Cumulative distribution data were analyzed by 2-sample Kolmogorov-Smirnov test, average data by Mann-Whitney test; n = 10 per group, $p > .05$ for all tests. **(A–C)** Data are expressed as mean ± SEM.

activate corticostriatal fibers and evoke EPSCs in striatal SPNs. Glutamatergic synaptic transmission was recorded in the presence of 50-μM picrotoxin at a holding potential of −60 mV (L5 CPNs) or −80 mV (SPNs). Miniature EPSCs were recorded the presence of 1-μM tetrodotoxin. GABAergic synaptic transmission was recorded at a holding potential of −35 mV and in the presence of 10-μM cyanquixaline and 10-μM AP-5. Electrophysiological data were acquired by an AxoPatch 200B amplifier and pClamp 10.2 software (Molecular Devices, Wokingham, United Kingdom). Series and input resistance were continuously monitored by sending 5-mV pulses, and neurons showing ≥20% change in these parameters were discarded from the analysis.

Statistical analysis was performed by Prism 7 (GraphPad Software, San Diego, CA). Two-tailed Mann-Whitney test was used for comparing two datasets, two-tailed Kruskal-Wallis and Dunn's post-test was used for comparing ≥3 datasets, 2-sample Kolmogorov-Smirnov test was used for comparing cumulative distributions, and one- and two-way analysis of variance was used for multiple comparisons. Sample size (n) refers to the number of recorded neurons. The significance threshold was fixed at $p < .05$. Tests used, p values, and n are indicated in the figures. Data are expressed as mean ± SEM.

Behavioral Testing

Male mice 101 to 127 days old were maintained in a social enriched environment and tested blind to the genotype for ASD-like criteria (11). Stereotypy scores were 1) the burying score obtained with marbles (36) and 2) the number of repeated dips in a hole board (37). A small number of crossed zones in an open field indicated a narrow field of interest (20). Sociability and interest in social novelty were measured in a two-chamber task (20,38) adapted from the three-chamber task (39). Although not included in DSM-5 criteria, anxiety, intellectual disability, and motor disorders are observed in 42% to 56%, ~45%, and ≤79%, respectively, of ASD patients (40). The presence of these symptoms was assessed by the elevated plus maze (20), Morris water maze, and notched bar

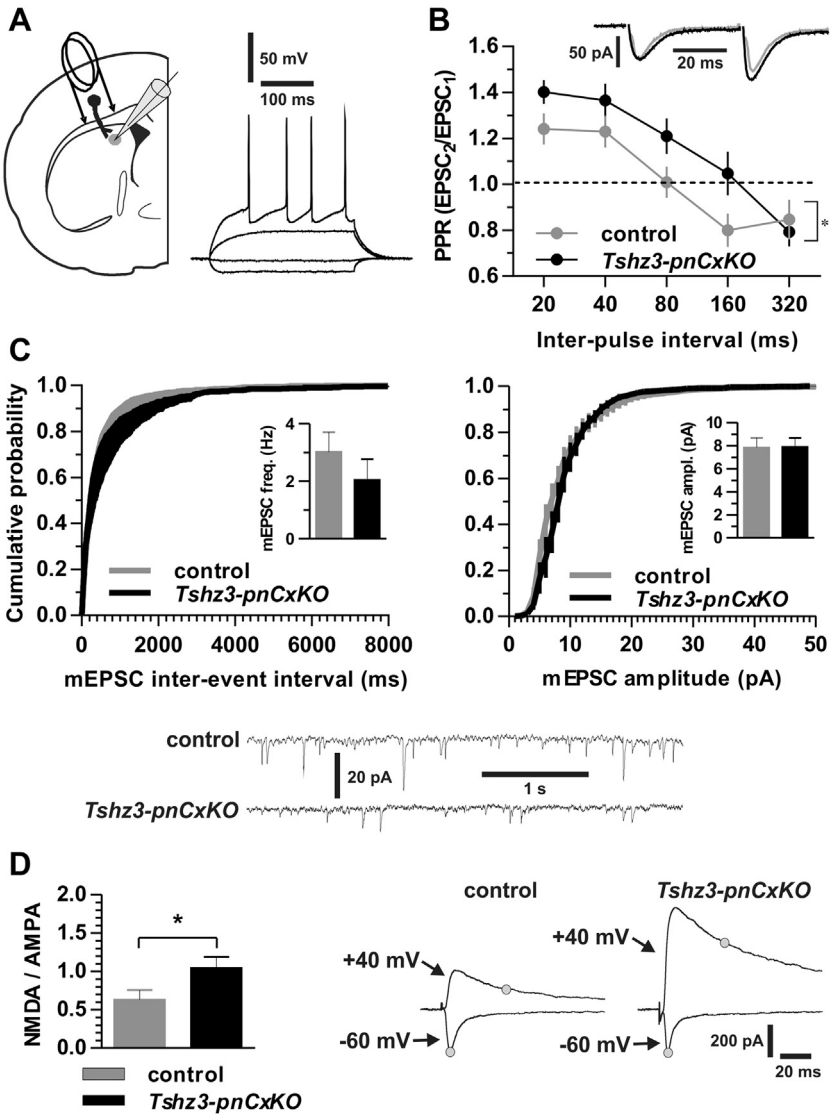

Figure 4. Corticostriatal synaptic transmission. **(A)** Scheme of a corticostriatal slice with a layer 5 cortical projection neuron (black) and a striatal spiny projection neuron (SPN) (gray), as well as the stimulating and recording electrodes. Traces depict the typical response of an SPN to the injection of hyperpolarizing (−200 pA) and depolarizing (+200, +400 pA) currents. **(B)** The paired-pulse ratio of corticostriatal glutamatergic excitatory postsynaptic currents (EPSCs) is significantly higher in SPNs of conditional mutant mice with postnatal loss of *Tshz3* in the cortex (*Tshz3-pnCxKO*) (n = 15) compared with control mice (n = 21) ($F_{1,87}$ = 5.7, p = .0182, two-way analysis of variance). Traces depict superimposed EPSCs (amplitude is normalized to control $EPSC_1$) recorded from SPNs of control and mutant mice. *p = .0182. **(C)** Cumulative distributions of miniature EPSC (mEPSC) interevent interval and amplitude (graphs), as well as frequency and amplitude (insets), are similar in SPNs of control and *Tshz3-pnCxKO* mice (n = 8 for both; 2-sample Kolmogorov-Smirnov and Mann-Whitney test, $p >$ .05 for all). Traces show sample mEPSCs. **(D)** The *N*-methyl-D-aspartate (NMDA)/alpha-amino-3-hydroxy-5-methyl-4-isoxazole propionic acid (AMPA) ratio is significantly higher in SPNs from *Tshz3-pnCxKO* compared with control mice (n = 8 for both; $p <$ .05, Mann-Whitney test). Traces depict sample EPSCs recorded at −60 and +40 mV to reveal the AMPA and NMDA receptor–mediated component, respectively (gray dots show where currents were measured). *$p <$ .05. **(B–D)** Data are expressed as mean ± SEM.

test (41), respectively. For further details and behavioral testing, see Supplement 1.

The assumption of statistical normality was checked. Analyses of covariance were conducted with genotype as independent variable and activity as covariate, for each score where the activity level must be controlled for. Repeated-measures analysis of covariance was used for testing sociability and social novelty. A two-tailed independent t test was used for the other comparisons. The results are expressed as effect size because the validation of an organism model for a disorder or a disease requires a significant difference and also a large (pathological) difference. Similar to previous articles, effect sizes are expressed as η^2 or partial η^2 as specified case by case, where values of .30 and .50 correspond to "mild impairment" and "impairment," respectively, by analogy with the intellectual disability field (40,41). Data are expressed as mean ± SEM.

Gene Set Enrichment Analysis

Preranked gene lists were calculated based on the $-\log_{10}$ of the p value from DESeq2 (https://bioconductor.org/) analysis multiplied by the sign of differential expression (Table S3T in Supplement 3). Gene matrix transposed (.gmt) files for Gene Ontology terms, as well as pathways, were downloaded from the Bader website (http://baderlab.org/GeneSets) (42). Data from the SynaptomeDB were received by the authors (43) and transformed into a .gmt file. Data from the Genes to Cognition (G2C) Synapse Proteomics Database were downloaded from the website (http://www.genes2cognition.org/proteomics/) (44) and transformed into a .gmt file. We performed Gene Set Enrichment Analysis (GSEA) using the software provided by the Broad Institute (45,46) with default parameters. For SynaptomeDB, as well as G2C Synapse Proteomics data, we also used the WebGestalt webserver (http://www.webgestalt.org/

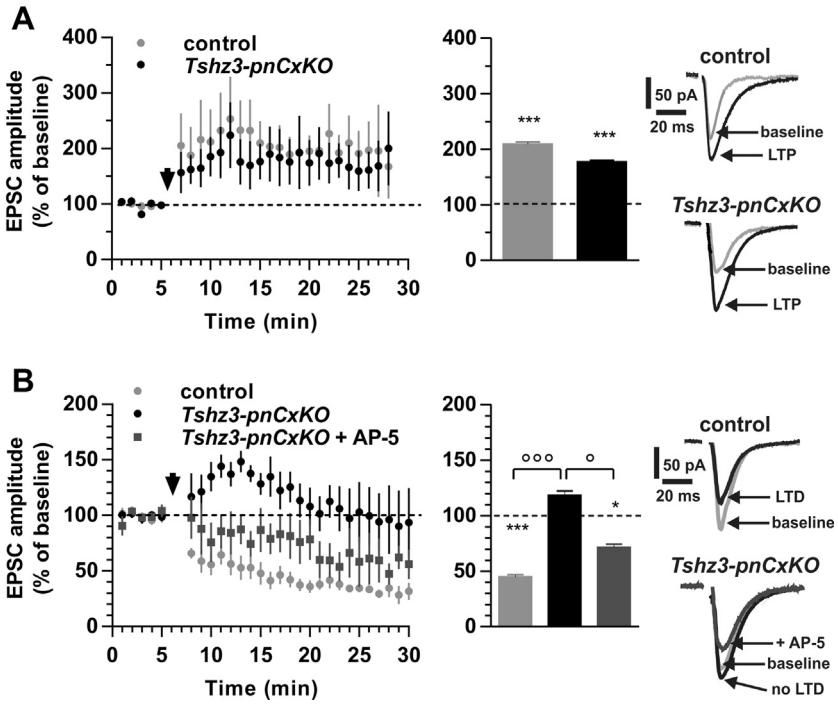

Figure 5. Corticostriatal synaptic plasticity. **(A)** Long-term potentiation (LTP) is similar in spiny projection neurons from conditional mutant mice with postnatal loss of *Tshz3* in the cortex (*Tshz3-pnCxKO*) and control mice (n = 10 and 7, respectively). The left graph shows the time course of excitatory postsynaptic current (EPSC) amplitude normalized to baseline (black arrow represents LTP induction protocol). The right histogram shows normalized EPSC amplitude after the LTP induction protocol ($p < .001$ compared with baseline, Mann-Whitney test). Traces depict sample EPSCs at baseline and 15 minutes after the LTP induction protocol (as indicated). ***$p <$ .001. **(B)** Long-term depression (LTD) is present in control spiny projection neurons (n = 10), while it is absent in *Tshz3-pnCxKO* mice (n = 11), where a transient potentiation is observed. The application of 40-μM AP-5 abolishes the transient potentiation and partially restores LTD (n = 7). Sample traces depict EPSCs at baseline and 15 minutes after LTD induction protocol in the different experimental conditions (as indicated). Note the absence of LTD in *Tshz3-pnCxKO* mice and its recovery by AP-5. *$p < .05$, ***$p < .001$ compared with baseline, Mann-Whitney test; °$p < .05$, °°°$p < .001$ between groups, Kruskal-Wallis and Dunn's post-test. **(A, B)** Data are expressed as mean ± SEM.

option.php) (47). Network of GSEA enrichments was produced using Cytoscape (48).

Accession Codes

Raw data (FastQ files) from the sequencing experiment (triplicates from wild-type and *Tshz3*-mutant cortices) and raw abundance measurements for genes (read counts) for each sample are available from Gene Expression Omnibus under accession GSE119791, which should be quoted in any manuscript discussing the data.

RESULTS

Morphological Characterization of Conditional *Tshz3* Knockout Mice

Analysis of TSHZ3 expression in *Tshz3-pnCxKO* mice at P28 (a time allowing strong Cre expression and recombination, as well as brain maturation) showed almost complete loss of this protein in the neocortex (Figure S1A, B in Supplement 1). Using the corticostriatal circuit as a model system, we evidenced it by cholera toxin subunit B retrograde tracing: the ipsi- and contralateral components of the corticostriatal projections were present in *Tshz3-pnCxKO* mice as in control mice (Figure S1C–F in Supplement 1). Labeling of NeuN (49) and BCL11B/CTIP2 (50), a neuron-specific and an L5/6-selective marker, respectively, was similar in both groups, further suggesting that the postnatal loss of *Tshz3* affects neither the number of cortical neurons nor their layering (Figure S1G–L in Supplement 1). In *Thy1-GFP-M;Tshz3-pnCxKO* mice, we did not observe major changes in the overall CPN morphology and projections (Figure S2 in Supplement 1), confirming the lack of major morphological defects after postnatal *Tshz3* loss. *Thy1-GFP-M;Tshz3-pnCxKO* mice were also used for Sholl analysis of L5 CPN dendrite morphology, revealing no major changes between control and mutant mice (Figure S3 in Supplement 1). However, we found a significantly reduced spine density in L5 CPNs (Figure 1), in agreement with other ASD-related mouse models (51). Finally, the density of vesicular glutamate transporter 1 staining was similar in control and *Thy1-GFP-M;Tshz3-pnCxKO* mice (Figure S4 in Supplement 1), suggesting unchanged density of corticostriatal terminals.

Electrophysiological Properties of L5 CPNs

The two main subtypes of L5 CPNs, pyramidal tract (PT) and intratelencephalic (IT) CPNs, were distinguished according to their electrophysiological properties (see Supplement 1), in particular the sum of the "sag & rebound" + the after-hyperpolarization responses (Figure 2B), whose value is larger in PT neurons (52). This "sag & rebound" + after-hyperpolarization sum was similar in control and *Tshz3-pnCxKO* mice (Figure 2C), indicating no major changes in membrane properties of CPNs and in the proportion of PT versus IT neurons. Other membrane and action potential (AP) properties were similar comparing IT versus PT neurons of the same genotype, as well as between PT and IT neurons of control versus *Tshz3-pnCxKO* mice (Table S1 in Supplement 1). Moreover, also comparing AP discharge patterns of PT versus IT neurons of the same genotype revealed no significant differences (Figure S6 in Supplement 1). We thus pooled PT and IT neurons of each genotype for further analyses. CPNs from *Tshz3-pnCxKO* mice showed a lower number of APs in response to depolarizing current pulses compared with control

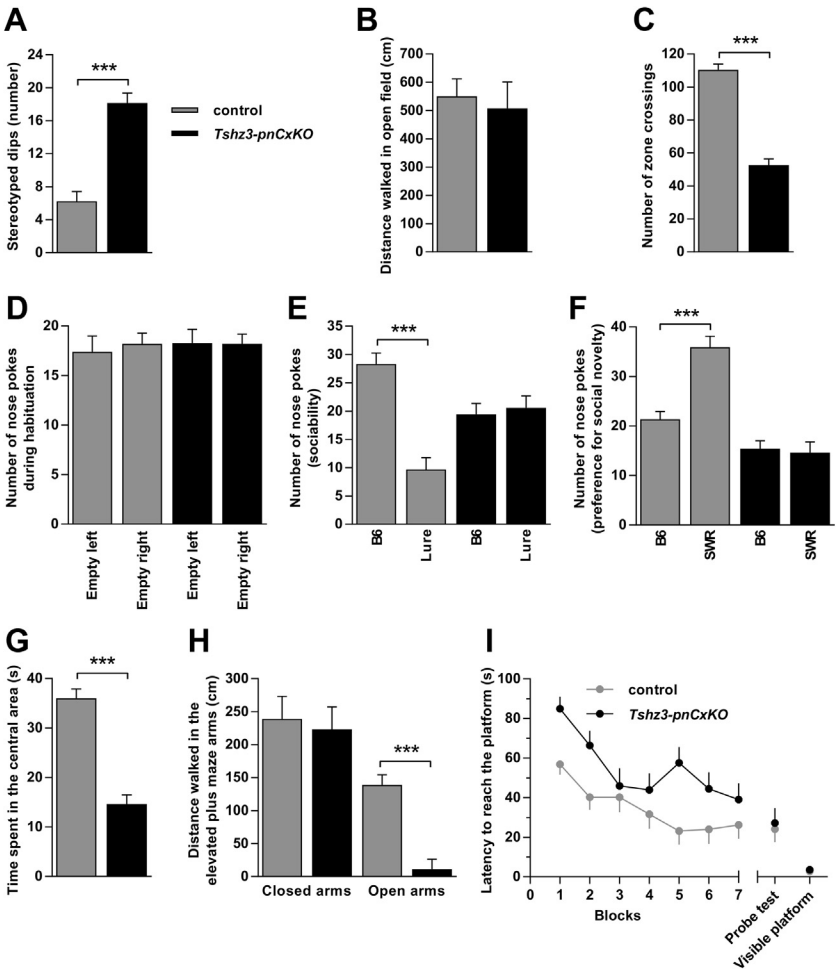

Figure 6. Stereotyped behavior, field of interest, sociability, interest in social novelty, anxiety-like behavior, and spatial learning. Conditional mutant mice with postnatal loss of *Tshz3* in the cortex (*Tshz3-pnCxKO*) displayed more stereotyped behaviors than control mice: **(A)** they dipped more repeatedly in the hole board ($F_{1,17}$ = 45.98, $p = 6 \times 10^{-6}$; partial η^2 = .73) when controlled for non-stereotyped dips (see Figure S7A, B in Supplement 1). **(B, C)** *Tshz3-pnCxKO* mice showed reduced field of interest with smaller number of zone crossing in the open field when controlled for distance walked ($F_{1,17}$ = 124.59, $p = 3 \times 10^{-9}$, partial η^2 = .88; covariate: distance walked, which was similar in the two groups [t_{18} = 0.39, p = .70, Cohen's d = 0.17]). Concerning sociability, *Tshz3-pnCxKO* mice did not differ in exploration from control mice **(D)**, but they did not show more contacts with conspecific C57BL/6J mice than **(E)** with a lure or **(F)** with a new SWR mouse vs. the familiar C57BL/6J mouse. Two repeated-measures analyses of covariance were designed. The interactions between the genotype and the content of the pencil box were significant in each condition **(D–F)** (condition B6 vs. lure [$F_{1,17}$= 31.75, p = .00003, partial η^2 = .65], condition B6 vs. SWR mouse [$F_{1,17}$ = 30.83, p = .00003, partial η^2 = .65; covariate: exploration level, panel **(D)**]). Control mice explored more the box containing a C57BL/6J than that containing a lure (dependent [t_9 = 12.48; $p = 3 \times 10^{-7}$; η^2 = .52]), and the box containing the SWR mouse more than that containing the familiar C57BL/6J animal (dependent [t_9 = 8.10; p = .00002; η^2 = .58]). In contrast, *Tshz3-pnCxKO* mice did not show more contacts with a conspecific C57BL/6J mouse than with a lure (dependent [t_9 = 0.39, p = .71]), or with the new SWR vs. the familiar C57BL/6J mouse (dependent [t_9 = 0.41, p = .69]). **(G)** *Tshz3-pnCxKO* mice showed more anxiety-like behavior: they avoided more the central area in the open field ($F_{1,17}$ = 124.59, $p = 3 \times 10^{-9}$; partial η^2 = .88; covariate: distance walked) when controlled for distance walked. **(H)** *Tshz3-pnCxKO* mice avoided also the open arms of the elevated plus maze when controlled for distance walked in the closed arms ($F_{1,17}$ = 36.41, p = .00001, partial η^2 = .68; covariate: activity in closed arms). **(I)** Both groups learned in a spatial task (Morris water maze): neither the learning slopes nor the probe score differed (t_{19} = 0.53, p = .60, and t_{19} = 0.30, p = .77, respectively); note that "visible platform" dots partially overlap. In all cases except one (marble burying), the effect size of the differences is large (see Results). **(A)** n = 11 per group. **(B–H)** n = 10 per group. **(K)** n = 9 per *Tshz3-pnCxKO* mouse and n = 12 per control mouse. **(K)** $^*p < .01$, $^{***}p < .0001$; data are expressed as mean ± SEM.

mice, although values were not significantly different (Figure 2D). The inter-AP interval in response to a strong depolarizing current (+300 pA) was also similar (Figure 2E). However, when measuring this parameter in response to a threshold current step (+150 pA, just above the rheobase), we found that the inter-AP intervals were significantly longer in CPNs from *Tshz3-pnCxKO* mice, suggesting increased accommodation and, possibly, decreased excitability (Figure 2F).

Cortical Synaptic Transmission

The paired-pulse ratio of AMPA receptor-mediated EPSCs recorded in L5 CPNs was significantly higher in *Tshz3-pnCxKO* CPNs compared with control CPNs (Figure 3A), suggesting a decreased probability of AP-dependent glutamate release from L2/3 cortical neurons. In contrast, the paired-pulse ratio of GABAergic inhibitory postsynaptic currents was similar in both genotypes (Figure 3B). Concerning AP-independent spontaneous activity, the distribution of miniature EPSC interevent interval and amplitude, as well as the average frequency and amplitude (Figure 3C), were similar in *Tshz3-pnCxKO* and control mice. Finally, the NMDA/AMPA ratio was also similar between control and mutant (0.69 ± 0.11, n = 22 vs. 0.51 ± 0.08, n = 20; p = .296, Mann-Whitney test).

Corticostriatal Synaptic Transmission and Plasticity

In the mouse, the bulk of the corticostriatal pathway is constituted by axons of L5 CPNs reaching the striatum around P3 to P4 and forming synapses from P10 onward (53). Their main targets are SPNs, which constitute >90% of the whole striatal neuronal population and do not express TSHZ3 (20). These facts and the implication of the corticostriatal pathway in ASD (10)

make this circuit (Figure 4A) a valuable tool for investigating the functional consequences of *Tshz3* loss in CPNs.

Striatal SPNs recorded from control (n = 16) and *Tshz3-pnCxKO* (n = 22) mice presented similar resting membrane potential and current–voltage relationship (not shown). Interestingly, the paired-pulse ratio was significantly higher in *Tshz3-pnCxKO* mice (Figure 4B), suggesting a decreased probability of AP-dependent glutamate release from L5 CPNs. Conversely, miniature EPSC parameters were not changed in *Tshz3-pnCxKO* compared with control mice (Figure 4C). Furthermore, in *Tshz3-pnCxKO* mice, the NMDA/AMPA ratio was significantly increased (Figure 4D).

Concerning synaptic plasticity, long-term potentiation (LTP) was present in both control and mutant mice (Figure 5A). Conversely, long-term depression (LTD) was absent in *Tshz3-pnCxKO* mice and was even reversed as a transient potentiation (Figure 5B). Interestingly, the blockade of NMDA receptors by AP-5 (40 μM) partially recovered LTD and abolished the transient potentiation (Figure 5B), suggesting that the lack of LTD could be due, at least in part, to increased NMDA receptor–mediated signaling.

ASD-Relevant Behavior

Tshz3-pnCxKO mice displayed more stereotyped behaviors than control mice: they buried more marbles and dipped more repeatedly in the hole board (Figure 6A and Figure S7A, B in Supplement 1). *Tshz3-pnCxKO* mice showed reduced field of interest with smaller number of zone crossing in the open field (Figure 6B, C) and also had lower sociability and lower interest in social novelty, as revealed by the two-chamber test (Figure 6D–F). In addition, *Tshz3-pnCxKO* mice showed increased anxiety-like behavior: they avoided the central area more in the open field (Figure 6B, G), as well as the open arms of the elevated plus maze (Figure 6H). Mutant and control mice learned equally in the Morris water maze (see Supplement 1): neither the learning slopes nor the probe scores differed, and the visible platform values were identical in the two groups (Figure 6I). The loss of *Tshz3* did not modify the hind paw coordination (2.0 ± 0.36 vs. 1.78 ± 0.52 hind paw slips for control mice vs. *Tshz3-pnCxKO* mice; n = 9 per group [t_{16} = 0.87, p = .39]). Finally, mutant mice did not show visual, auditory, and olfactory deficits (Figure S7C–E in Supplement 1).

Genes Differentially Expressed in the *Tshz3-pnCxKO* Cerebral Cortex Are Strongly Associated With ASD

RNA sequencing, performed at P28 in the cortex of *Tshz3-pnCxKO* and control mice, identified 1025 differentially expressed genes (DEGs), among which 767 were upregulated and 258 downregulated ($p < .05$) (Table S2A in Supplement 2). A total of 993 of these DEGs have nonambiguous human orthologues (Table S2B in Supplement 2). GSEA showed consistent negative or positive enrichment of Gene Ontology terms associated with neurological and synaptic functions/pathways, as well as neurological disorders, such as ASD and Alzheimer's disease (Figure 7A, B; Table S3A–X in Supplement 3). GSEA from the SynaptomeDB [http://metamoodics.org/SynaptomeDB/index.php (43)] and from the G2C postsynaptic proteome datasets [http://www.genes2cognition.org/proteomics (44)] revealed positive enrichment of *postsynaptic*, *presynaptic*, and *presynaptic active zone* and negative enrichment for *vesicle* Gene Ontology terms (Figure 7C; Table S3L–O in Supplement 3). Interestingly, we found a strong enrichment for the NMDA receptor pathway, while few genes were related to the AMPA receptor pathway (Figure 7C). Of the 1025 DEGs, 173 (16.7%) encode for postsynaptic density (PSD) proteins from the adult mouse cerebral cortex, among which 167 have human orthologues (54) (Table S2B–D in Supplement 2). Interestingly, among these 167 proteins, 28 were identified as components of the DLG4, DLGAP1, and/or SHANK3 postsynaptic protein-interaction networks of the adult mouse cortex (55) (Table S2E in Supplement 2).

Last, of the 993 human orthologues, 741 (74.6%) are involved in brain and nervous system disorders. Among these 741 genes, 489 (66%) are known or proposed to be involved in ASD (Table S2F, G in Supplement 2). Note that the percentage of ASD-associated genes remains high when restricting the analysis to the 357 human orthologues of the 382 DEGs having an absolute value of $\log_2$ fold change >0.5 and the adjusted p value (or false discovery rate) $<.05$ (Table S2H in Supplement 2). In this condition, 155 (43.4%) genes of 357 are associated with ASD, among which 13 (*GRIN2A*, *GRIN2B*, *MIF*, *MYH6*, *MYH14*, *NDUFA13*, *NOS1*, *PHGDH*, *PRR7*, *PURA*, *RFTN1*, *SYT2*, *VGF*) encode for PSD proteins (Figure 7D; Table S2H–K in Supplement 2).

DISCUSSION

In our previous work (20), we showed a direct link between *TSHZ3* loss and ASD and reported dramatic changes in gene expression in the fetal neocortex (E18.5) of *Tshz3*$^{-/-}$ mice, with 243 DEGs.

Here, transcriptomic analysis of *Tshz3-pnCxKO* mice at P28 revealed a very different pattern and number of DEGs. Notably, there were 1025 DEGs, among which only 38 previously identified in *Tshz3*$^{-/-}$ (see Table S4 in Supplement 4), showing that TSHZ3 has different regulatory functions at prenatal versus postnatal stages. Interestingly, postnatal *Tshz3* loss also clearly leads to abnormal expression of 173 genes of the PSD, as well as 59 "presynaptic" genes such as *Nrxn2*, *Syt2*, and *Syn2* (Table S2L in Supplement 2) implicated in synapse adhesion and neurotransmitter release (56,57). Altogether, these results highlight a fascinating dual role of TSHZ3 in prenatal versus postnatal stages, confirming that it participates in different transcriptional programs dependent on the developmental stage. All these DEGs belong to a converging network in terms of human brain diseases: notably, in both cases, ASD first, and schizophrenia second, are the most represented pathologies associated to these genes. Consistently, we show here that *Tshz3-pnCxKO* mice display the whole set of ASD-like behavioral abnormalities, namely social interaction deficits, restricted fields of interest, and stereotypies, similarly to *Tshz3*$^{+/-}$ mice, a model mimicking the human pathology (20). Therefore, the alteration of different transcriptional programs resulting from *Tshz3* deficiency at embryonic or postnatal stages converges into a similar ASD phenotype. These data raise the issue of the contribution of postnatal events to the ASD phenotype of *Tshz3*$^{+/-}$ mice and call for future rescue experiments to test the hypothesis of an

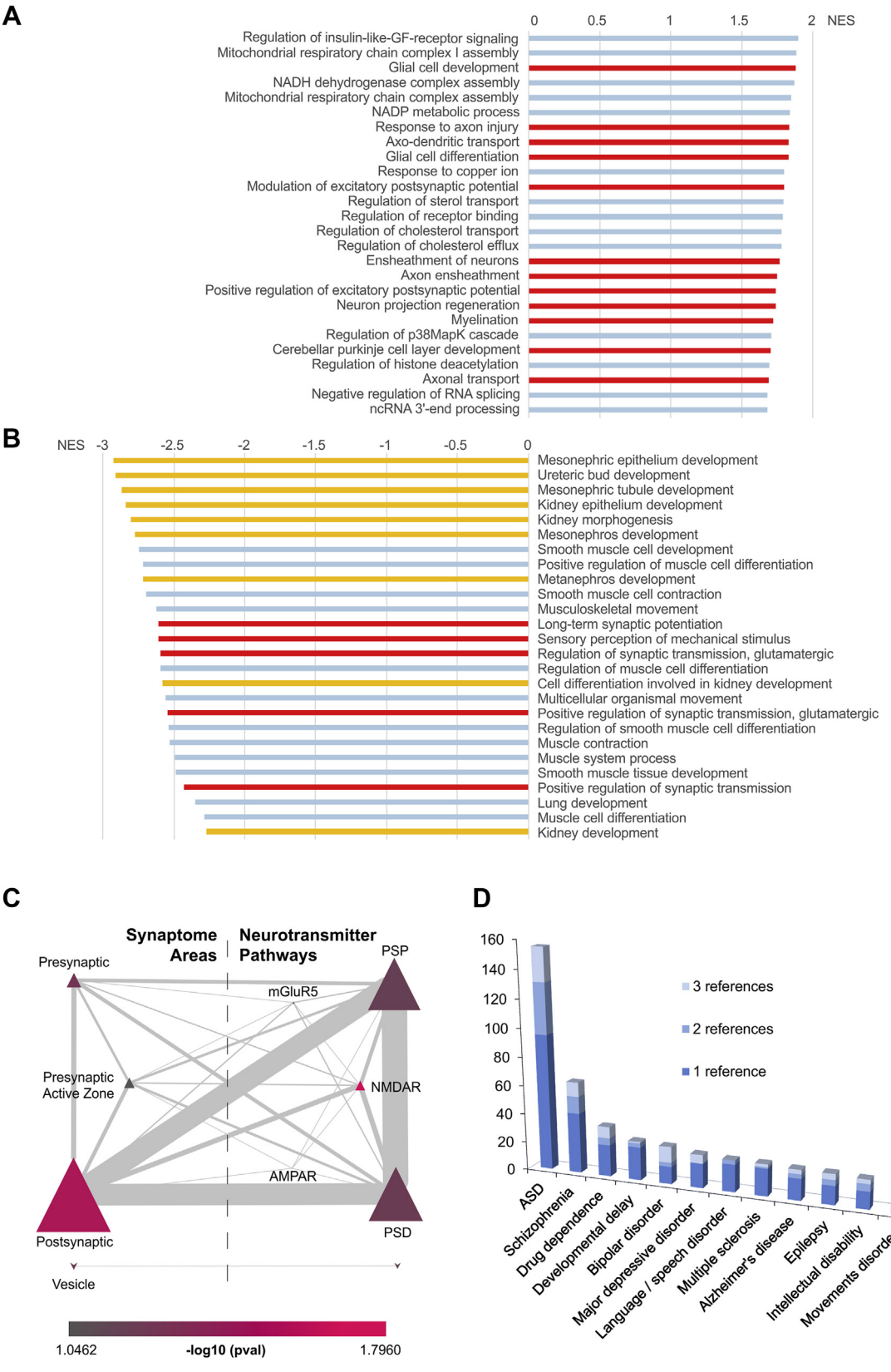
A
0
0.5
1
1.5
2
NES
Regulation of insulin-like-GF-receptor signaling
Mitochondrial respiratory chain complex I assembly
Glial cell development
NADH dehydrogenase complex assembly
Mitochondrial respiratory chain complex assembly
NADP metabolic process
Response to axon injury
Axo-dendritic transport
Glial cell differentiation
Response to copper ion
Modulation of excitatory postsynaptic potential
Regulation of sterol transport
Regulation of receptor binding
Regulation of cholesterol transport
Regulation of cholesterol efflux
Ensheathment of neurons
Axon ensheathment
Positive regulation of excitatory postsynaptic potential
Neuron projection regeneration
Myelination
Regulation of p38MapK cascade
Cerebellar purkinje cell layer development
Regulation of histone deacetylation
Axonal transport
Negative regulation of RNA splicing
ncRNA 3'-end processing
B
NES
-3
-2.5
-2
-1.5
-1
-0.5
0
Mesonephric epithelium development
Ureteric bud development
Mesonephric tubule development
Kidney epithelium development
Kidney morphogenesis
Mesonephros development
Smooth muscle cell development
Positive regulation of muscle cell differentiation
Metanephros development
Smooth muscle cell contraction
Musculoskeletal movement
Long-term synaptic potentiation
Sensory perception of mechanical stimulus
Regulation of synaptic transmission, glutamatergic
Regulation of muscle cell differentiation
Cell differentiation involved in kidney development
Multicellular organismal movement
Positive regulation of synaptic transmission, glutamatergic
Regulation of smooth muscle cell differentiation
Muscle contraction
Muscle system process
Smooth muscle tissue development
Positive regulation of synaptic transmission
Lung development
Muscle cell differentiation
Kidney development
C
Synaptome Areas
Neurotransmitter Pathways
Presynaptic
PSP
mGluR5
Presynaptic Active Zone
NMDAR
AMPAR
Postsynaptic
PSD
Vesicle
1.0462
-log10 (pval)
1.7960
D
160
140
120
100
80
60
40
20
0
3 references
2 references
1 reference
ASD
Schizophrenia
Drug dependence
Developmental delay
Bipolar disorder
Major depressive disorder
Language / speech disorder
Multiple sclerosis
Alzheimer's disease
Epilepsy
Intellectual disability
Movements disorder

early postnatal therapeutic window for the ASD-like syndrome linked to *TSHZ3* haploinsufficiency.

Mutations linked to ASD induce structural and functional changes in brain circuitry, including spine morphology/density, synaptic transmission, and plasticity (58), strongly involving the corticostriatal circuitry (7,10,59), suggesting that this pathway constitutes a main target for studying brain dysfunctions associated to this pathology. Accordingly, we reported functional abnormalities in the corticostriatal pathway associated with the ASD-related phenotype in *Tshz3*$^{+/-}$ mice (20). Consistently, here, we found that cortical AP-dependent glutamate release is significantly reduced in *Tshz3-pnCxKO* mice and that L5 CPNs have decreased spine density, which is usually associated to diminished synaptic activity (60), as well as slightly reduced excitability. L2/3 and L5 neurons normally express TSHZ3, and thus these changes could be attributed to a "direct" effect of postnatal *Tshz3* loss on their maturation and functioning as well as on the establishment of their synaptic network. In turn, the reduced AP-dependent glutamate release in the striatum could be interpreted as a consequence of the above-mentioned modifications at cortical level. In parallel, the increased NMDA/AMPA ratio measured in striatal SPNs could be interpreted as a compensatory mechanism: NMDA receptor signaling, which is crucial for synaptic plasticity (61), could be enhanced to compensate for the lower corticostriatal input. In this respect, the abnormal corticostriatal LTD reported here is particularly striking and fitting: LTD in the striatum can be induced in conditions limiting NMDA receptor activation; conversely, LTP induction requires their full activation (33,62–68). In this context, the exacerbated NMDA receptor–mediated signaling might lead to the observed loss of LTD and the transient LTP-like phenomenon; the partial recovery of LTD by NMDA receptor blockade strongly supports this hypothesis. Alternatively, or concomitantly, LTD loss could be attributed to an occlusion effect: as basal corticostriatal synaptic transmission is downregulated, it cannot be further depressed. Interestingly, changes in corticostriatal function have been evidenced in several mouse models of ASD (17–20). These alterations are heterogeneous, possibly owing to the different models, experimental protocols, and genetic backgrounds. However, they all strongly suggest that altered corticostriatal synaptic transmission/plasticity is a hallmark of ASD.

Long-lasting changes of synaptic strength can reinforce (LTP) or depress (LTD) specific neural circuits, thus gating salient information while suppressing unwanted ones to optimize behavioral responses (69). If, as in our case, one of the two forms of plasticity is altered or absent, these processes would be unpaired, contributing to the observed behavioral abnormalities. Whereas the molecular and anatomo-functional defects in corticostriatal circuitry could underlie at least part of the ASD-like features of *Tshz3-pnCxKO* mice, other brain circuits and structures might also be involved, such as those involving the medial prefrontal cortex and the basolateral amygdala (70), as TSHZ3 and CaMKIIalpha are expressed there (20,21,71). In agreement with the very low *Tshz3* expression in the hippocampus (21), *Tshz3-pnCxKO* mice have no memory deficit.

Overall, the above-mentioned molecular, functional, and morphological changes in CPNs due to *Tshz3* loss further support the current idea that ASD can be considered as a synaptopathy (70,72). Here, we show that several DEGs in *Tshz3-pnCxKO* mice are actually involved in glutamatergic synaptic transmission at both pre- and postsynaptic level, including genes involved in NMDA receptor signaling pathway, PSD-95, and SH3 and multiple ankyrin repeat domains protein complex. There is increasing evidence that NMDA receptor–dependent signaling pathway is involved not only in ASD, but also in Alzheimer's disease, while AMPA receptor–mediated signaling is relatively spared (73), leading to the hypothesis that *TSHZ3*-related ASD can be considered as a synaptopathy linked to NMDA receptor pathway abnormalities.

Here, we demonstrate that *Tshz3* plays an essential role in the cortex and in corticostriatal circuitry during postnatal development, which is different from that played at prenatal stages in terms of gene expression modulation. This supports the position of TSHZ3 as a critical neurodevelopmental regulator participating at differential age-related processes of gene transcription and confirms its role as an ASD-risk gene, providing new ASD models in rodents and pointing to dysfunctional corticostriatal circuitry as a substrate for this group of neurodevelopmental disorders.

ACKNOWLEDGMENTS AND DISCLOSURES

This work was supported by the French National Research Agency (ANR) "TSHZ3inASD" project Grant No. ANR-17-CE16-0030-01 (to LF, LK-LG, and BH); a grant from the Fédération pour la Recherche sur le Cerveau (FRC) (to LF); the Centre National de la Recherche Scientifique (CNRS), the Institut National de la Santé et de la Recherche Médicale (INSERM), and Aix Marseille Univ; "Investments for the Future" program (France-BioImaging) Grant No. ANR-10-INSB-04-01 (to the imaging platform of the IBDM); and "France Génomique" national infrastructure "Investissement d'Avenir" Grant No. ANR-10-INSB-09 (to DS and ED). IBDM and LPC are affiliated with Marseille NeuroSchool, a graduate school supported by the A*MIDEX foundation and the French ANR funded by the French Government "Investissements d'Avenir" program (nEURo*AMU, ANR-17-EURE-0029 grant).

Figure 7. Gene Set Enrichment Analysis (GSEA) enrichment. **(A)** Positive and **(B)** negative GSEA enrichment of the Gene Ontology category "Biological Process" using the preranked *Tshz3* gene list. The normalized enriched score (NES) value from the gene set enrichment is shown. Red color indicates neuro-related terms, orange color designates kidney-related terms, and all other terms are shown in light blue. **(C)** Network of GSEA enrichments of different synaptome areas and postsynaptic neurotransmitter pathways. The color of the nodes represents the $-\log_{10}$ of the *p* value (pval) from GSEA for each term, the size of the nodes roughly indicates the total number of genes found for each term based on the formula (number of genes/10) × 2. The strength of the interactions (line thickness) indicates shared genes between the terms. **(D)** Histogram showing the most represented human brain and nervous system pathologies associated with the 357 human orthologs of the 382 *Tshz3*-regulated differentially expressed genes (DEGs) with $\log_2$ fold change >0.5 and *p* value (or false discovery rate) <.05. Each gene is scored on the basis of the number of relevant publications that associate it with a pathology. Scores were given as follows: 1, one publication; 2, two publications; 3, >2 publications. AMPAR, alpha-amino-3-hydroxy-5-methyl-4-isoxazole propionic acid receptor; ASD, autism spectrum disorder; GF, growth factor; mGluR5, metabotropic glutamate receptor 5; NADH, nicotinamide adenine dinucleotide; NADP, nicotinamide adenine dinucleotide phosphate; ncRNA, noncoding RNA; NMDAR, *N*-methyl-D-aspartate receptor; PSD, postsynaptic density; PSP, postsynaptic potential.

We wish to thank Dr. Francis Castet and Dr. Jean-Pierre Kessler (IBDM) for, respectively, performing some experiments and his kind advice on NMDA receptors.

The authors report no biomedical financial interests or potential conflicts of interest.

ARTICLE INFORMATION

From the Aix Marseille Univ, CNRS, IBDM (DC, XC, BH, BJ, PS, MM, AF, LK-LG, LF, PG), the Aix Marseille Univ, CNRS, LPC (MC), the Aix Marseille Univ, INSERM, MMG (PLR), and the Aix Marseille Univ, INSERM, TAGC (BH), Marseille, France; the Max Delbrück Center for Molecular Medicine (CF) and the Institute of Cell Biology and Neurobiology, Center for Anatomy, Charité University Hospital Berlin (ANG), Berlin, Germany; and the Univ Montpellier, CNRS, INSERM, MGX (DS, ED), Montpellier, France.

DC and XC contributed equally to this work as joint first authors.

LK-LG, LF, and PG contributed equally to this work as joint senior authors.

Address correspondence to Paolo Gubellini, Ph.D., IBDM, UMR7288 CNRS/Aix-Marseille Université, Case 907, Campus de Luminy, 13009 Marseille, France; E-mail: paolo.gubellini@univ-amu.fr; or Laurent Fasano, Ph.D., IBDM, UMR7288 CNRS/Aix-Marseille Université, Case 907, Campus de Luminy, 13009 Marseille, France; E-mail: laurent.fasano@univ-amu.fr.

Received Oct 30, 2018; revised and accepted Mar 7, 2019.

Supplementary material cited in this article is available online at https://doi.org/10.1016/j.biopsych.2019.03.974.

REFERENCES

1. DeLong MR, Wichmann T (2007): Circuits and circuit disorders of the basal ganglia. Arch Neurol 64:20–24.
2. Levy R, Hazrati LN, Herrero MT, Vila M, Hassani OK, Mouroux M, *et al.* (1997): Re-evaluation of the functional anatomy of the basal ganglia in normal and Parkinsonian states. Neuroscience 76:335–343.
3. Redgrave P, Vautrelle N, Reynolds JN (2011): Functional properties of the basal ganglia's re-entrant loop architecture: Selection and reinforcement. Neuroscience 198:138–151.
4. Willsey AJ, Sanders SJ, Li M, Dong S, Tebbenkamp AT, Muhle RA, *et al.* (2013): Coexpression networks implicate human midfetal deep cortical projection neurons in the pathogenesis of autism. Cell 155:997–1007.
5. Parikshak NN, Luo R, Zhang A, Won H, Lowe JK, Chandran V, *et al.* (2013): Integrative functional genomic analyses implicate specific molecular pathways and circuits in autism. Cell 155:1008–1021.
6. State MW, Sestan N (2012): Neuroscience. The emerging biology of autism spectrum disorders. Science 337:1301–1303.
7. Delmonte S, Gallagher L, O'Hanlon E, McGrath J, Balsters JH (2013): Functional and structural connectivity of frontostriatal circuitry in autism spectrum disorder. Front Hum Neurosci 7:430.
8. Langen M, Bos D, Noordermeer SD, Nederveen H, van Engeland H, Durston S (2014): Changes in the development of striatum are involved in repetitive behavior in autism. Biol Psychiatry 76:405–411.
9. Langen M, Schnack HG, Nederveen H, Bos D, Lahuis BE, de Jonge MV, *et al.* (2009): Changes in the developmental trajectories of striatum in autism. Biol Psychiatry 66:327–333.
10. Shepherd GM (2013): Corticostriatal connectivity and its role in disease. Nat Rev Neurosci 14:278–291.
11. American Psychiatric Association (2013): Diagnostic and Statistical Manual of Mental Disorders, 5th ed. Washington, DC: American Psychiatric Press.
12. Bourgeron T (2016): Current knowledge on the genetics of autism and propositions for future research. C R Biol 339:300–307.
13. Buxbaum JD, Daly MJ, Devlin B, Lehner T, Roeder K, State MW, Autism Sequencing C (2012): The autism sequencing consortium: large-scale, high-throughput sequencing in autism spectrum disorders. Neuron 76:1052–1056.
14. Park HR, Lee JM, Moon HE, Lee DS, Kim BN, Kim J, *et al.* (2016): A short review on the current understanding of autism spectrum disorders. Exp Neurobiol 25:1–13.
15. Ziats MN, Rennert OM (2016): The evolving diagnostic and genetic landscapes of autism spectrum disorder. Front Genet 7:65.
16. Peixoto RT, Wang WG, Croney DM, Kozorovitskiy Y, Sabatini BL (2016): Early hyperactivity and precocious maturation of corticostriatal circuits in Shank3B(−/−) mice. Nature Neuroscience 19:716–724.
17. Peca J, Feliciano C, Ting JT, Wang W, Wells MF, Venkatraman TN, *et al.* (2011): Shank3 mutant mice display autistic-like behaviours and striatal dysfunction. Nature 472:437–442.
18. Blundell J, Blaiss CA, Etherton MR, Espinosa F, Tabuchi K, Walz C, *et al.* (2010): Neuroligin-1 deletion results in impaired spatial memory and increased repetitive behavior. J Neurosci 30:2115–2129.
19. Portmann T, Yang M, Mao R, Panagiotakos G, Ellegood J, Dolen G, *et al.* (2014): Behavioral abnormalities and circuit defects in the basal ganglia of a mouse model of 16p11.2 deletion syndrome. Cell Rep 7:1077–1092.
20. Caubit X, Gubellini P, Andrieux J, Roubertoux PL, Metwaly M, Jacq B, *et al.* (2016): TSHZ3 deletion causes an autism syndrome and defects in cortical projection neurons. Nat Genet 48:1359–1369.
21. Caubit X, Tiveron MC, Cremer H, Fasano L (2005): Expression patterns of the three Teashirt-related genes define specific boundaries in the developing and postnatal mouse forebrain. J Comp Neurol 486:76–88.
22. Li M, Santpere G, Imamura Kawasawa Y, Evgrafov OV, Gulden FO, Pochareddy S, *et al.* (2018): Integrative functional genomic analysis of human brain development and neuropsychiatric risks. Science 362:eaat7615.
23. Caubit X, Thoby-Brisson M, Voituron N, Filippi P, Bevengut M, Faralli H, *et al.* (2010): Teashirt 3 regulates development of neurons involved in both respiratory rhythm and airflow control. J Neurosci 30:9465–9476.
24. Kang HJ, Kawasawa YI, Cheng F, Zhu Y, Xu X, Li M, *et al.* (2011): Spatio-temporal transcriptome of the human brain. Nature 478:483–489.
25. Workman AD, Charvet CJ, Clancy B, Darlington RB, Finlay BL (2013): Modeling transformations of neurodevelopmental sequences across mammalian species. J Neurosci 33:7368–7383.
26. Tepper JM, Sharpe NA, Koos TZ, Trent F (1998): Postnatal development of the rat neostriatum: Electrophysiological, light- and electron-microscopic studies. Dev Neurosci 20:125–145.
27. Kwan KY, Sestan N, Anton ES (2012): Transcriptional co-regulation of neuronal migration and laminar identity in the neocortex. Development 139:1535–1546.
28. Wang H, Cuzon VC, Pickel VM (2003): Postnatal development of mu-opioid receptors in the rat caudate-putamen nucleus parallels asymmetric synapse formation. Neuroscience 118:695–708.
29. Inaji M, Sato K, Momose-Sato Y, Ohno K (2011): Voltage-sensitive dye imaging analysis of functional development of the neonatal rat corticostriatal projection. Neuroimage 54:1831–1839.
30. Mullah SH, Inaji M, Nariai T, Momose-Sato Y, Sato K, Ohno K (2012): Optical analysis of developmental changes in synaptic potentiation in the neonatal rat corticostriatal projection. Neuroscience 201:338–348.
31. Feng G, Mellor RH, Bernstein M, Keller-Peck C, Nguyen QT, Wallace M, *et al.* (2000): Imaging neuronal subsets in transgenic mice expressing multiple spectral variants of GFP. Neuron 28:41–51.
32. Rodriguez A, Ehlenberger DB, Dickstein DL, Hof PR, Wearne SL (2008): Automated three-dimensional detection and shape classification of dendritic spines from fluorescence microscopy images. PLoS One 3:e1997.
33. Chassain C, Melon C, Salin P, Vitale F, Couraud S, Durif F, *et al.* (2016): Metabolic, synaptic and behavioral impact of 5-week chronic deep brain stimulation in hemiparkinsonian rats. J Neurochem 136:1004–1016.
34. Jiang ZG, North RA (1991): Membrane properties and synaptic responses of rat striatal neurones in vitro. J Physiol 443:533–553.
35. Hattox AM, Nelson SB (2007): Layer V neurons in mouse cortex projecting to different targets have distinct physiological properties. J Neurophysiol 98:3330–3340.

36. Thomas A, Burant A, Bui N, Graham D, Yuva-Paylor LA, Paylor R (2009): Marble burying reflects a repetitive and perseverative behavior more than novelty-induced anxiety. Psychopharmacology 204:361–373.
37. Makanjuola RO, Hill G, Maben I, Dow RC, Ashcroft GW (1977): An automated method for studying exploratory and stereotyped behaviour in rats. Psychopharmacology (Berl) 52:271–277.
38. Roubertoux PL, Carlier M, Tordjman S (2015): Deficit in social relationships and reduced field of interest in mice. In: Roubertoux PL, editor. Deficit in Social Relationships and Reduced Field of Interest in Mice. New York: Springer, 335–370.
39. Moy SS, Nadler JJ, Perez A, Barbaro RP, Johns JM, Magnuson TR, *et al.* (2004): Sociability and preference for social novelty in five inbred strains: An approach to assess autistic-like behavior in mice. Genes Brain Behav 3:287–302.
40. Lai MC, Lombardo MV, Baron-Cohen S (2014): Autism. Lancet 383:896–910.
41. Roubertoux PL, Baril N, Cau P, Scajola C, Ghata A, Bartoli C, *et al.* (2017): Differential brain, cognitive and motor profiles associated with partial trisomy. modeling down syndrome in mice. Behav Genet 47:305–322.
42. Merico D, Isserlin R, Stueker O, Emili A, Bader GD (2010): Enrichment map: A network-based method for gene-set enrichment visualization and interpretation. PLoS One 5:e13984.
43. Pirooznia M, Wang T, Avramopoulos D, Valle D, Thomas G, Huganir RL, *et al.* (2012): SynaptomeDB: An ontology-based knowledgebase for synaptic genes. Bioinformatics 28:897–899.
44. Collins MO, Husi H, Yu L, Brandon JM, Anderson CN, Blackstock WP, *et al.* (2006): Molecular characterization and comparison of the components and multiprotein complexes in the postsynaptic proteome. J Neurochem 97(suppl 1):16–23.
45. Subramanian A, Tamayo P, Mootha VK, Mukherjee S, Ebert BL, Gillette MA, *et al.* (2005): Gene set enrichment analysis: A knowledge-based approach for interpreting genome-wide expression profiles. Proc Natl Acad Sci U S A 102:15545–15550.
46. Mootha VK, Lindgren CM, Eriksson KF, Subramanian A, Sihag S, Lehar J, *et al.* (2003): PGC-1alpha-responsive genes involved in oxidative phosphorylation are coordinately downregulated in human diabetes. Nat Genet 34:267–273.
47. Wang J, Vasaikar S, Shi Z, Greer M, Zhang B (2017): WebGestalt 2017: A more comprehensive, powerful, flexible and interactive gene set enrichment analysis toolkit. Nucleic Acids Res 45:W130–W137.
48. Su G, Morris JH, Demchak B, Bader GD (2014): Biological network exploration with Cytoscape 3. Curr Protoc Bioinformatics 47:8.13.1–8.13.24.
49. Mullen RJ, Buck CR, Smith AM (1992): NeuN, a neuronal specific nuclear protein in vertebrates. Development 116:201–211.
50. Arlotta P, Molyneaux BJ, Chen J, Inoue J, Kominami R, Macklis JD (2005): Neuronal subtype-specific genes that control corticospinal motor neuron development in vivo. Neuron 45:207–221.
51. Lai KO, Ip NY (2013): Structural plasticity of dendritic spines: The underlying mechanisms and its dysregulation in brain disorders. Biochim Biophys Acta 1832:2257–2263.
52. Lee AT, Gee SM, Vogt D, Patel T, Rubenstein JL, Sohal VS (2014): Pyramidal neurons in prefrontal cortex receive subtype-specific forms of excitation and inhibition. Neuron 81:61–68.
53. Sohur US, Padmanabhan HK, Kotchetkov IS, Menezes JR, Macklis JD (2014): Anatomic and molecular development of corticostriatal projection neurons in mice. Cereb Cortex 24:293–303.
54. Bayes A, Collins MO, Croning MD, van de Lagemaat LN, Choudhary JS, Grant SG (2012): Comparative study of human and mouse postsynaptic proteomes finds high compositional conservation and abundance differences for key synaptic proteins. PLoS One 7:e46683.
55. Li J, Zhang W, Yang H, Howrigan DP, Wilkinson B, Souaiaia T, *et al.* (2017): Spatiotemporal profile of postsynaptic interactomes integrates components of complex brain disorders. Nat Neurosci 20:1150–1161.
56. Weingarten J, Lassek M, Mueller BF, Rohmer M, Lunger I, Baeumlisberger D, *et al.* (2014): The proteome of the presynaptic active zone from mouse brain. Mol Cell Neurosci 59:106–118.
57. Zhang W, Zhang Y, Zheng H, Zhang C, Xiong W, Olyarchuk JG, *et al.* (2007): SynDB: A Synapse protein DataBase based on synapse ontology. Nucleic Acids Res 35:D737–D741.
58. Bourgeron T (2015): From the genetic architecture to synaptic plasticity in autism spectrum disorder. Nat Rev Neurosci 16:551–563.
59. Maloney SE, Rieger MA, Dougherty JD (2013): Identifying essential cell types and circuits in autism spectrum disorders. Int Rev Neurobiol 113:61–96.
60. Sekino Y, Kojima N, Shirao T (2007): Role of actin cytoskeleton in dendritic spine morphogenesis. Neurochem Int 51:92–104.
61. Fino E, Paille V, Cui Y, Morera-Herreras T, Deniau JM, Venance L (2010): Distinct coincidence detectors govern the corticostriatal spike timing-dependent plasticity. J Physiol 588:3045–3062.
62. Calabresi P, Maj R, Pisani A, Mercuri NB, Bernardi G (1992): Long-term synaptic depression in the striatum: Physiological and pharmacological characterization. J Neurosci 12:4224–4233.
63. Calabresi P, Pisani A, Mercuri NB, Bernardi G (1992): Long-term potentiation in the striatum is unmasked by removing the voltage-dependent magnesium block of Nmda receptor channels. Eur J Neurosci 4:929–935.
64. Lovinger DM, Tyler EC, Merritt A (1993): Short- and long-term synaptic depression in rat neostriatum. J Neurophysiol 70:1937–1949.
65. Partridge JG, Tang KC, Lovinger DM (2000): Regional and postnatal heterogeneity of activity-dependent long-term changes in synaptic efficacy in the dorsal striatum. J Neurophysiol 84:1422–1429.
66. Lovinger DM (2010): Neurotransmitter roles in synaptic modulation, plasticity and learning in the dorsal striatum. Neuropharmacology 58:951–961.
67. Bagetta V, Picconi B, Marinucci S, Sgobio C, Pendolino V, Ghiglieri V, *et al.* (2011): Dopamine-dependent long-term depression is expressed in striatal spiny neurons of both direct and indirect pathways: Implications for Parkinson's disease. J Neurosci 31:12513–12522.
68. Paille V, Picconi B, Bagetta V, Ghiglieri V, Sgobio C, Di Filippo M, *et al.* (2010): Distinct levels of dopamine denervation differentially alter striatal synaptic plasticity and NMDA receptor subunit composition. J Neurosci 30:14182–14193.
69. Berretta N, Nistico R, Bernardi G, Mercuri NB (2008): Synaptic plasticity in the basal ganglia: A similar code for physiological and pathological conditions. Prog Neurobiol 84:343–362.
70. Wang X, Kery R, Xiong Q (2018): Synaptopathology in autism spectrum disorders: Complex effects of synaptic genes on neural circuits. Prog Neuropsychopharmacol Biol Psychiatry 84:398–415.
71. Casanova E, Fehsenfeld S, Mantamadiotis T, Lemberger T, Greiner E, Stewart AF, Schutz G (2001): A CamKIIalpha iCre BAC allows brain-specific gene inactivation. Genesis 31:37–42.
72. Reig-Viader R, Sindreu C, Bayes A (2018): Synaptic proteomics as a means to identify the molecular basis of mental illness: Are we getting there? Prog Neuropsychopharmacol Biol Psychiatry 84:353–361.
73. Lepeta K, Lourenco MV, Schweitzer BC, Martino Adami PV, Banerjee P, Catuara-Solarz S, *et al.* (2016): Synaptopathies: Synaptic dysfunction in neurological disorders - A review from students to students. J Neurochem 138:785–805.